2024 IEEE International Conference on Robotics and Automation (ICRA 2024)
May 13-17, 2024. Yokohama, Japan

Trajectory-prediction-based Dynamic Tracking of a UGV to a Moving Target under Multi-disturbed Conditions

Jinge Si, Bin Li, Yongkang Xu, Liang Wang, Chencheng Deng, Shoukun Wang, and Junzheng Wang

***Abstract*— Tracking dynamic targets poses a significant challenge for Unmanned Ground Vehicles (UGVs). Existing methods often lack research on multi-disturbed conditions. To address this issue, we propose a trajectory-prediction-based dynamic tracking scheme, which includes target localization, trajectory prediction, and UGV control. Firstly, an estimation algorithm based on the Extended Kalman Filter (EKF) is employed to mitigate noise and estimate the absolute states of the target accurately. To enhance robustness, we present an Adaptive Trajectory Prediction (ATP) algorithm based on prediction anchors. In this method, a quantization standard for trajectory disturbance is designed for adaptive control. Subsequently, we iteratively solve prediction anchor points based on two motion models to robustly predict the target trajectory even in the presence of unknown disturbances. Finally, the Linear Time-Varying Model Predictive Control (LTV-MPC) is utilized in the UGV controller for dynamic tracking. Experimental results demonstrate that the ATP exhibits superior prediction robustness and accuracy in perturbed environments compared to other prediction algorithms. In addition, the proposed scheme effectively achieves dynamic tracking of the Unmanned Aerial Vehicle (UAV) by the UGV under multi-disturbed conditions. Specifically, when the target moves at a speed of 1.0 m/s, the UGV can maintain a tracking error within 0.346 m.**

I. INTRODUCTION

The study of tracking dynamic targets has garnered considerable attention across various platforms, such as Unmanned Aerial Vehicles (UAVs) [1], underwater robots [2], and robot arms [3]. Most of the existing research assumes the presence of precise reference localization or trajectory information for the tracking system [4]. However, obtaining such data accurately in real-world scenarios often poses significant challenges, particularly for non-cooperative targets.

The tracking methods for dynamic targets without available reference states are generally categorized into behavior-based and prediction-based approaches [5]. In the former, a feedback loop is established in the controller at the sensor level to detect and track the target [6], [7]. Consequently, these methods exhibit limited transient responses, rendering them suitable only for targets with minimal motion changes and disturbances [8], [9].

In prediction-based method, the target state is predicted based on historical observations, providing a tracking reference for the system [10]. Sun *et al*. [11] developed a neuroadaptive tracking control scheme embedded with memory-based trajectory predictor for unknown targets. In [4], the target trajectory was reconstructed and predicted through an artificial neural network for the tracking system under conditions of modeling uncertainties and actuation faults. These prediction-based approaches offer enhanced robustness by providing more comprehensive tracking references compared to behavior-based approaches. As a result, they are more commonly applied for tracking disturbed targets [12], [13].

The authors are with the State Key Laboratory of Intelligent Control and Decision of Complex System, Beijing Institute of Technology, School of Automation, Beijing, China. bit_si_jin_ge@bit.edu.cn, lb18801318201@163.com, yongkang.xu@ieee.org, yanqianyi_liang@bit.edu.cn, dengcc@bit.edu.cn, bitwsk@bit.edu.cn, wangjz@bit.edu.cn

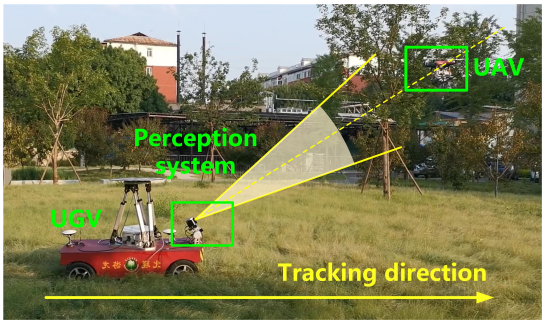

Fig. 1. A dynamic target tracking experiment.

In this study, we introduce a trajectory-prediction-based dynamic tracking scheme specifically designed for Unmanned Ground Vehicles (UGVs) to track drones under challenging multi-disturbed conditions. The proposed scheme includes state estimation and trajectory prediction algorithms to effectively counteract the impact of disturbances, significantly enhancing the system's robustness.

A. Related Work

In related works, disturbances primarily consist of two types: 1. in perception, the sensor detection noise and frame rate fluctuations lead to the unavailability of UAV location; 2. during target prediction, the UAV trajectory may fluctuate violently due to crosswinds, making it challenging to provide accurate tracking references for the vehicles.

In prediction-based methods, the accuracy of target localization directly influences the precision of prediction and tracking [14], [15]. For the first type of disturbance, Wang *et al*. [16] designed an Extended Kalman filter (EKF) that combines different sensors to enable real-time tracking of humans in Three Dimensions (3D) by robots. Paral *et al*. [17] developed a feature-based extended target tracking system via multisensor information fusion, potentially decreasing the observation noise. However, in practical engineering, observing targets under conditions of high detection noise remains a significant challenge for current research. In some cases, the system may encounter difficulties in capturing the

target states for tracking, especially when the observation is affected by noise pollution and frame rate fluctuations [18].

After obtaining the target's state estimation, the system needs to predict the target's motion to provide tracking reference for the vehicles [19], [20]. Sun *et al.* [21] proposed an online solution for reconstructing and predicting the uncertain target trajectory based on a General Regression Neural Network (GRNN) to chase the uncertain target. In [22], a novel trajectory prediction method using Gaussian Processes (GPs) was developed to correct environmental disturbances. To improve prediction accuracy, Li *et al.* [23] designed a Multi-step Unscented Kalman Filter (MUKF) to forecast the multi-step trajectory in different regions. However, the target trajectory often faces random disturbances in practical applications, and most current research focuses on improving prediction accuracy rather than robustness [24]. Therefore, these methods are hard to implement for target motion prediction under such challenging conditions.

B. Our Contribution

In our work, we have achieved dynamic tracking of the moving UAV by the UGV under multiple disturbance scenarios. This paper presents the following main contributions:

1) We propose an Adaptive Trajectory Prediction (ATP) algorithm. Specifically, we design a standard to quantize trajectory disturbances. Then, the system adaptively recursively solves for prediction anchor points based on two models. By incorporating points into the curve fitting, the system can accurately and robustly predict the trajectory of a disturbed UAV as a stable reference for UGV tracking.
2) A trajectory-prediction-based dynamic tracking scheme is introduced, including the EKF for state estimation, the APF for target prediction, and the Linear Time-Varying Model Predictive Control (LTV-MPC) for UGV tracking. Experiments demonstrate the effective tracking of moving targets by the UGV under multi-disturbed conditions.

II. PROBLEM FORMULATION

A. Predefinition

We first define specific coordinate frames to facilitate the description as shown in Fig. 2. Σ_G, Σ_B, and Σ_T denote the global frame, the UGV body frame, and the turntable frame, respectively. The origin of each frame is represented by points $O_i, (i \in G, B, T)$. Note that we have chosen the plane positioning data converted to Σ_T as the observation input instead of the original 3D lidar data to simplify the calculations of coordinate conversions.

In this paper, the subscript and pre-superscript respectively represent the object and coordinate frame of variables. For instance, the drone's localization in the turntable frame, Σ_T, is described by ${}^T\boldsymbol{P}_D = \left[{}^T x_D, {}^T y_D\right]^T$. To enhance readability, we omit the pre-superscript for variables defined within the global framework. In addition, the rotation matrix ${}^i\boldsymbol{R}_j \, (i, j \in \{G, B, T\})$ is employed to describe the transformation from the frame Σ_j to Σ_i. Specifically,

$$ {}^B\boldsymbol{R}_T = \begin{bmatrix} \cos{}^B\theta_T & -\sin{}^B\theta_T \\ \sin{}^B\theta_T & \cos{}^B\theta_T \end{bmatrix}, \tag{1} $$

where ${}^B\theta_T = \theta_T - \theta_B$ denotes the heading angle of the turntable in Σ_B.

B. Systematic Observation Model

To reduce the impact of observation noise on the system, we use the EKF algorithm to estimate the target position. In this section, we derive the system's observation model by analyzing the motion and coordinate transformation of the vehicle. Firstly, we provide the kinematic model of the UGV with front and rear axle steering as follows.

$$ \begin{aligned} \dot{x}_B &= v_B \cos\theta_B + \xi_{x_B} \\ \dot{y}_B &= v_B \sin\theta_B + \xi_{y_B} \\ \dot{\theta}_B &= \frac{2v_B \tan\delta_B}{L} + \xi_{\theta_B}, \end{aligned} \tag{2} $$

where $\boldsymbol{P}_B = [x_B, y_B]^T$ represents the position of the UGV in X and Y directions, θ_B denotes the vehicle's heading

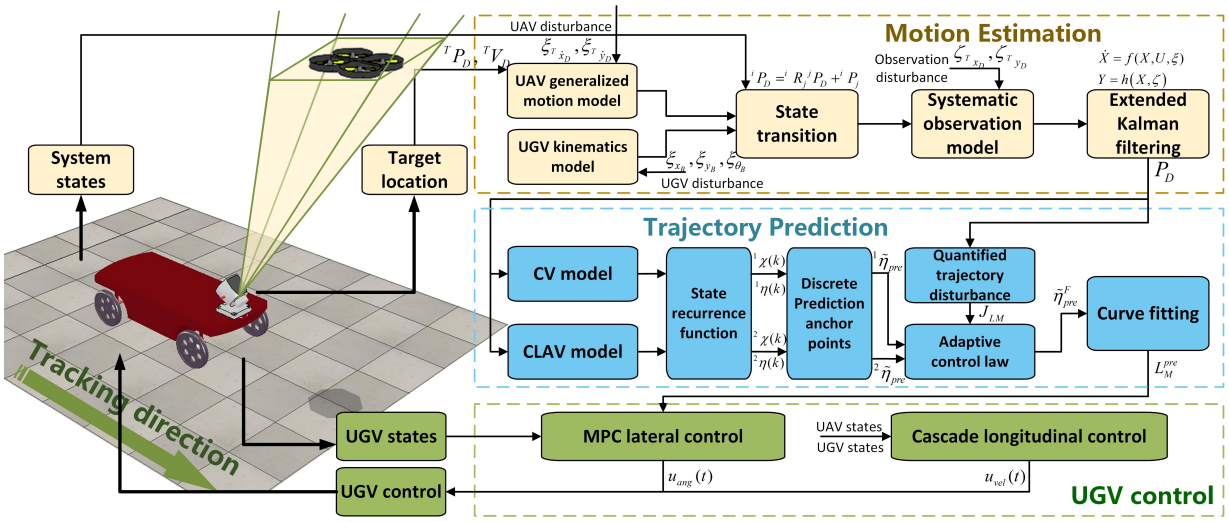

Fig. 2. The control structure of the system.

angle, v_B, δ_B, and L are the control speed, steering angle, and wheelbase of the UGV, ξ_{x_B}, ξ_{y_B}, and ξ_{θ_B} are the mutually independent random variables standing for additive process noise of the system states.

In addition, establishing a generalized velocity model for the non-cooperative target in Σ_T as

$$ {}^T\dot{\boldsymbol{P}}_D = \begin{bmatrix} {}^T\dot{x}_D + \xi_{{}^T\dot{x}_D} \\ {}^T\dot{y}_D + \xi_{{}^T\dot{y}_D} \end{bmatrix}, \tag{3} $$

where ${}^T\boldsymbol{P}_D = \left[{}^Tx_D, {}^Ty_D\right]^T$ represents the drone's position, $\xi_{{}^T\dot{x}_D}$ and $\xi_{{}^T\dot{y}_D}$ denote the corresponding additive process noise.

Furthermore, to achieve target tracking in Σ_G, the positions of the UAV in UGV frame ${}^B\boldsymbol{P}_D$ and in global frame $\boldsymbol{P}_D$ are calculated through its relative location ${}^T\boldsymbol{P}_D$ in turntable frame, as shown below.

$$ \begin{aligned} {}^B\boldsymbol{P}_D &= {}^B\boldsymbol{R}_T {}^T\boldsymbol{P}_D + {}^B\boldsymbol{P}_T \\ \boldsymbol{P}_D &= \boldsymbol{R}_B {}^B\boldsymbol{P}_D + \boldsymbol{P}_B, \end{aligned} \tag{4} $$

where ${}^B\boldsymbol{P}_T$ and $\boldsymbol{P}_B$ denote the positions of the turntable in Σ_B and the UGV in Σ_G, ${}^B\boldsymbol{R}_T$ and $\boldsymbol{R}_B$ indicate the rotation matrix from Σ_T to Σ_B and Σ_B to Σ_G.

As the turntable is fixed to the UGV, we set $\theta_T = \theta_B$, ${}^B\theta_T = 0$, and $\dot{\theta}_T = \dot{\theta}_B$. By taking the time derivative on both sides of the target absolute position and substituting Eq. (2) and Eq. (3), we have

$$ \begin{aligned} \dot{x}_D = &\left({}^T\dot{x}_D + \xi_{T\dot{x}_D}\right)\cos\theta_T - \left({}^T\dot{y}_D + \xi_{T\dot{y}_D}\right)\sin\theta_T \\ &- \left(\frac{2v_B\tan\delta_B}{L} + \xi_{\theta_B}\right)(y_D - y_B) + v_B\cos\theta_B + \xi_{x_B} \\ \dot{y}_D = &\left({}^T\dot{x}_D + \xi_{T\dot{x}_D}\right)\sin\theta_T + \left({}^T\dot{y}_D + \xi_{T\dot{y}_D}\right)\cos\theta_T \\ &+ \left(\frac{2v_B\tan\delta_B}{L} + \xi_{\theta_B}\right)(x_D - x_B) + v_B\sin\theta_B + \xi_{y_B}. \end{aligned} \tag{5} $$

Additionally, the relative location in Σ_T is deduced by Eq. (4) that ${}^T\boldsymbol{P}_D = {}^B\boldsymbol{R}_T^{-1}\left[\boldsymbol{R}_B^{-1}\left(\boldsymbol{P}_D - \boldsymbol{P}_B\right) - {}^B\boldsymbol{P}_T\right]$. The following observation equation is obtained as

$$ \begin{aligned} {}^Tx_D = &\cos\theta_T\left(x_D - x_B\right) + \sin\theta_T\left(y_D - y_B\right) \\ &- {}^Bx_T\cos{}^B\theta_T - {}^By_T\sin{}^B\theta_T + \zeta_{{}^Tx_D} \\ {}^Ty_D = &-\sin\theta_B\left(x_D - x_B\right) + \cos\theta_B\left(y_D - y_B\right) \\ &+ {}^Bx_T\sin{}^B\theta_T - {}^By_T\cos{}^B\theta_T + \zeta_{{}^Ty_D}. \end{aligned} \tag{6} $$

We define $\boldsymbol{X} = [x_D, y_D]^T$, $\boldsymbol{U} = [v_B, \delta_B]^T$, $\boldsymbol{\xi} = \left[\xi_{x_B}, \xi_{y_B}, \xi_{\theta_B}, \xi_{{}^T\dot{x}_D}, \xi_{{}^T\dot{y}_D}\right]^T$, $\boldsymbol{Y} = \left[{}^Tx_D, {}^Ty_D\right]$, and $\boldsymbol{\zeta} = \left[\zeta_{{}^Tx_D}, \zeta_{{}^Ty_D}\right]$. The measurement equation of the system is rewritten as follows.

$$ \begin{aligned} \dot{\boldsymbol{X}} &= f(\boldsymbol{X}, \boldsymbol{U}, \boldsymbol{\xi}) \\ \boldsymbol{Y} &= h(\boldsymbol{X}, \boldsymbol{\zeta}). \end{aligned} \tag{7} $$

In our works, the target absolute position x_D, y_D is utilized for motion prediction and tracking. However, these measurements are subject to noise and fluctuations in the frame rate. Therefore, the measured values ${}^Tx_D$ and ${}^Ty_D$ need to be processed further.

C. Vehicle Dynamic Model

In UGV controller, we adopt the following vehicle dynamics model [25] for control.

$$ \begin{aligned} \dot{y}_{\tilde{B}} &= -\dot{x}_{\tilde{B}}\dot{\theta}_B + \frac{2}{m}\left[C_{\mathrm{cf}}\left(\delta_B - \frac{\dot{y}_{\tilde{B}} + l_{\mathrm{f}}\dot{\theta}_B}{\dot{x}_{\tilde{B}}}\right) + C_{\mathrm{cr}}\left(-\delta_B - \frac{l_{\mathrm{r}}\dot{\theta}_B - \dot{y}_{\tilde{B}}}{\dot{x}_{\tilde{B}}}\right)\right] \\ \dot{x}_{\tilde{B}} &= \dot{y}_{\tilde{B}}\dot{\theta}_B + \frac{2}{m}\left[C_{\mathrm{lf}}s_{\mathrm{f}} + C_{\mathrm{lr}}s_{\mathbf{r}} + C_{\mathrm{cf}}\left(\delta_B - \frac{\dot{y}_{\tilde{B}} + l_{\mathrm{f}}\dot{\theta}_B}{\dot{x}_{\tilde{B}}}\right)\delta_B\right. \\ &\quad \left. - C_{\mathrm{cr}}\left(-\delta_B - \frac{l_{\mathbf{r}}\dot{\theta}_B - \dot{y}_{\tilde{B}}}{\dot{x}_{\tilde{B}}}\right)\delta_B\right] \\ \ddot{\theta}_B &= \frac{2}{I_{\mathrm{z}}}\left[l_{\mathrm{f}}C_{\mathrm{cf}}\left(\delta_B - \frac{\dot{y}_{\tilde{B}} + l_{\mathrm{f}}\dot{\theta}_B}{\dot{x}_{\tilde{B}}}\right) - l_{\mathrm{r}}C_{\mathrm{cr}}\left(-\delta_B - \frac{l_{\mathrm{r}}\dot{\theta}_B - \dot{y}_{\tilde{B}}}{\dot{x}_{\tilde{B}}}\right)\right] \\ \dot{y}_B &= \dot{x}_{\tilde{B}}\sin\theta_B + \dot{y}_{\tilde{B}}\cos\theta_B \\ \dot{x}_B &= \dot{x}_{\tilde{B}}\cos\theta_B - \dot{y}_{\tilde{B}}\sin\theta_B, \end{aligned} \tag{8} $$

where $\dot{x}_{\tilde{B}}$ and $\dot{y}_{\tilde{B}}$ indicate the velocity components of the UGV along the X and Y axes of Σ_B, I_{z} and m denote the rotational inertia in the Z direction and the weight of the vehicle. l_i and $s_i\,(i \in \{f, r\})$ respectively indicate the wheelbase and the slip ratio of the front and rear wheels, $C_{ji}\,(j \in \{l, c\}, i \in \{f, r\})$ denote the longitudinal slip and the cornering stiffness of the front and rear wheels respectively.

III. PROPOSED APPROACH

This study addresses the limitations associated with dynamic target tracking in complex scenarios by implementing the following methods: (1) designing an EKF-based estimation algorithm to precisely determine the target's location; (2) developing an APF algorithm utilizing the location to generate stable predicted trajectories for jittery targets; (3) employing the LTV-MPC on the UGV to accurately track the target based on the predicted trajectory. The system's control structure is depicted in Fig. 2.

A. Target localization

In this section, a probabilistic target localization algorithm based on EKF is designed to filter the severe detection noise and compensate for the lost data frames, which can provide more accurate estimates of the target's position in Σ_G.

It's assumed that the probability distribution functions of the measurement noise and the process noise fit the normal distributions, and the initial state $\hat{\boldsymbol{X}}_0^+ = [x_D(0), y_D(0)]^T$ is known. The absolute position of the UAV is estimated recursively by an EKF-based algorithm as follows.

$$ \begin{aligned} \hat{\boldsymbol{X}}_k^- &= f_{k-1}\left(\hat{\boldsymbol{X}}_{k-1}^+, \boldsymbol{U}_{k-1}, \boldsymbol{0}\right) \\ \boldsymbol{E}_k^- &= \boldsymbol{F}_{k-1}\boldsymbol{E}_{k-1}^+\boldsymbol{F}_{k-1}^T + \boldsymbol{L}_{k-1}\boldsymbol{Q}_{k-1}\boldsymbol{L}_{k-1}^T \\ \boldsymbol{K}_k &= \boldsymbol{E}_k^-\boldsymbol{H}_k^T\left[\boldsymbol{H}_k\boldsymbol{E}_k^-\boldsymbol{H}_k^T + \boldsymbol{M}_k\boldsymbol{R}_k\boldsymbol{M}_k^T\right]^{-1} \\ \hat{\boldsymbol{X}}_k^+ &= \begin{cases} \hat{\boldsymbol{X}}_k^- + \boldsymbol{K}_k\left[\boldsymbol{Y}_k - h_k\left(\hat{\boldsymbol{X}}_k^-, \boldsymbol{0}\right)\right] & \text{if } \boldsymbol{Y}_k \text{ exists} \\ \hat{\boldsymbol{X}}_k^- & \text{otherwise} \end{cases} \\ \boldsymbol{E}_k^+ &= \left[\boldsymbol{I} - \boldsymbol{K}_k\boldsymbol{H}_k\right]\boldsymbol{E}_k^-\left[\boldsymbol{I} - \boldsymbol{K}_k\boldsymbol{H}_k\right]^T + \boldsymbol{K}_k\boldsymbol{R}_k\boldsymbol{K}_k^T, \end{aligned} \tag{9} $$

where $\boldsymbol{X}_k = f_{k-1}\left(\boldsymbol{X}_{k-1}, \boldsymbol{U}_{k-1}, \boldsymbol{\xi}_{k-1}\right)$ and $\boldsymbol{Y}_k = h_k\left(\boldsymbol{X}_k, \boldsymbol{\zeta}_k\right)$ are the discretized observation equation based

on Eq. (7), $\boldsymbol{F}$, $\boldsymbol{L}$, $\boldsymbol{H}$, and $\boldsymbol{M}$ denote the partial derivative matrix of the linearized measurement equation.

From Eq. (9), we estimate the UAV position $\hat{\boldsymbol{X}}_k^+ = [\hat{x}_D(k), \hat{y}_D(k)]^T$ to reduce the effects of detection noise and data loss, providing reliable real-time target states as the reference for subsequent prediction and tracking.

B. Target Trajectory Prediction

In practical applications, the target trajectory often jitters due to various disturbances, such as crosswind and auxiliary positioning deviation. This jitter poses challenges for algorithms to accurately and stably predict target trajectories, consequently affecting the tracking performance of UGVs. To address this issue, we propose the ATP based on the predicted anchor points through state updating to improve the robustness of trajectory prediction. This algorithm employs curve fitting without relying on learning algorithms. Consequently, it is easy to deploy and enables real-time tracking.

The insufficient quantitative analysis makes it challenging for prediction algorithms to handle disturbances in the trajectory, resulting in significant deviations when the algorithm encounters a disturbed trajectory [26]. Regarding this issue, we propose a quantization standard for trajectory disturbance used for adaptive control before initiating the prediction.

Select N_L discrete positioning points in the current and the past time to form the target trajectory $\boldsymbol{L}_M$ as below.

$$\boldsymbol{L}_M = \left\{ \hat{\boldsymbol{X}}_{k-N_L+1}^+, \hat{\boldsymbol{X}}_{k-N_L+2}^+, \cdots, \hat{\boldsymbol{X}}_k^+ \right\}. \tag{10}$$

We employ polynomials to fit the trajectory based on the least square. The trajectory function f_{LM} is obtained that

$$\begin{aligned} f_{LM}\left(\hat{x}_D(i)\right) &= w_0 + w_1 \hat{x}_D(i) + \ldots + w_M \hat{x}_D^M(i) \\ &= \sum w_j \hat{x}_D^j(i), \end{aligned} \tag{11}$$

where w is the coefficient of each order in polynomial fitting, $i \in \{k - N_L + 1, \cdots, k\}$.

By considering the deviation of each point from the fitting curve, we define the following evaluation function J_{LM} for quantitative assessment.

$$J_{LM}(k) = \sqrt{\sum_{i=k-N_L+1}^{k} \left(\frac{H + \left(f_{LM}\left(\hat{x}_D(i)\right) - \hat{y}_D(i)\right)^2}{H + k - N_L - i} \right)}, \tag{12}$$

where H is a constant, and the index i of each point represents its weight. As the value of i increases, the point becomes closer to the current state, and its weight correspondingly increases.

Based on the disturbance analysis of historical trajectories, corresponding state space equations are designed for the trajectories of characteristic features to represent the target's motion patterns under specific conditions. The system recursively predicts the target states as anchor points through these equations.

We categorize trajectory characteristics into two groups: with and without disturbance. For trajectories without disturbance, we approximate the target as a motion model with Constant Longitudinal and Angular Velocity (CLAV). We set the initial state vector as $\hat{\boldsymbol{x}}_{k_0}^+ = [\hat{x}_D(k_0), \hat{y}_D(k_0)]^T$. The corresponding system model is shown as follows.

$$\begin{aligned} \dot{x}_{pre}(k) &= v \cos\theta_{pre} + \nu_{x1} \\ \dot{y}_{pre}(k) &= v \sin\theta_{pre} + \nu_{y1} \\ \dot{\theta}_{pre}(k) &= \omega + \xi_\theta, \end{aligned} \tag{13}$$

where v and ω denote the longitudinal velocity and heading angular velocity of the model, which are fitted by $\boldsymbol{L}_M$, ν_{x1} and ν_{y1} represent the state prediction bias in CLAV.

For trajectories with severe disturbances, we design a generalized Constant Velocity (CV) model for updating to maintain the stability of the predicted trajectory.

$$\begin{aligned} \dot{x}_{pre}(k) &= v_x(k_0 - (k - k_0)) + \nu_{x2} \\ \dot{y}_{pre}(k) &= v_y(k_0 - (k - k_0)) + \nu_{y2}, \end{aligned} \tag{14}$$

where v_x and v_y are the velocities of the motion in X and Y directions at time $T = k_0 - (k - k_0)$, ν_{x2} and ν_{y2} indicate the state prediction bias in CV.

After linearization and discretization, Eq. (13) and (14) are rewritten as the following discrete state recurrence functions.

$$\begin{aligned} {}^i\boldsymbol{\chi}(k) &= {}^i\boldsymbol{F}\left[{}^i\boldsymbol{\chi}(k-1)\right] + {}^i\boldsymbol{\nu}_\chi(k) \\ {}^i\boldsymbol{\eta}(k) &= {}^i\boldsymbol{C}\boldsymbol{\chi}(k) + {}^i\boldsymbol{\nu}_\eta(k), \end{aligned} \tag{15}$$

where $i \in [1, 2]$ denotes two types of recurrence, ${}^i\boldsymbol{F}$ represents the recursive functions of two motion models, ${}^i\boldsymbol{C}$ is the output matrix that converts the predicted states of the motion model ${}^i\boldsymbol{\chi}$ to absolute coordinates ${}^i\boldsymbol{\eta} = [x_D^{pre}, y_D^{pre}]^T$, ${}^i\boldsymbol{\nu}_\chi$ and ${}^i\boldsymbol{\nu}_\eta$ represent the state prediction bias matrix. We select part of discrete time points within prediction time N_p.

$$\boldsymbol{N} = [k_0, k_0 + N_p/N_x, k_0 + 2N_p/N_x, \cdots, k_0 + N_p]^T, \tag{16}$$

where N_x is the interval coefficient. For the motion described in Eq. (15), the recursive prediction of the two motion models over the future horizon N_P is

$$\begin{aligned} &{}^i\tilde{\boldsymbol{\eta}}_{pre}(k_0 + N_p|k_0) = \\ &\begin{bmatrix} {}^i\boldsymbol{\eta}(k_0) \\ {}^i\boldsymbol{\eta}(k_0 + N_p/N_x) \\ {}^i\boldsymbol{\eta}(k_0 + 2N_p/N_x) \\ \vdots \\ {}^i\boldsymbol{\eta}(k_0 + N_p) \end{bmatrix} = \begin{bmatrix} {}^i\boldsymbol{C}\,{}^i\hat{\boldsymbol{\chi}}(k_0) \\ {}^i\boldsymbol{C}\,{}^i\boldsymbol{F}^{N_p/N_x}\left[{}^i\hat{\boldsymbol{\chi}}(k_0)\right] \\ {}^i\boldsymbol{C}\,{}^i\boldsymbol{F}^{2N_p/N_x}\left[{}^i\hat{\boldsymbol{\chi}}(k_0)\right] \\ \vdots \\ {}^i\boldsymbol{C}\,{}^i\boldsymbol{F}^{N_p}\left[{}^i\hat{\boldsymbol{\chi}}(k_0)\right] \end{bmatrix}, \end{aligned} \tag{17}$$

where ${}^i\tilde{\boldsymbol{\eta}}_{pre}$ indicates two points set of recursive prediction, ${}^i\boldsymbol{F}^j$ is denoted as the function ${}^i\boldsymbol{F}$ undergoing j iterations.

Combining the prediction evaluation function in Eq. (12) and two prediction point sets in Eq. (17), we derive the set of adaptive predicted anchor points $\tilde{\boldsymbol{\eta}}_{pre}^F(k_0 + N_p|k)$ as

$$\tilde{\boldsymbol{\eta}}_{pre}^F(k_0 + N_p|k) = \sum_{i=1}^{2} J_{pre}(i)\,{}^i\boldsymbol{C}\,{}^i\tilde{\boldsymbol{\eta}}_{pre}(k_0 + N_p|k), \tag{18}$$

where $J_{pre} = \left\{ \frac{J_{\max} - J_{LM}(k)}{J_{\max} - J_{\min}}, \frac{J_{LM}(k) - J_{\min}}{J_{\max} - J_{\min}} \right\}$, and the set with predicted anchor points for the ATP is given as follows.

$$L_M^{pre} = \left\{ L_M, \tilde{\boldsymbol{\eta}}_{pre}^F(k_0 + N_p|k) \right\}. \tag{19}$$

Ultimately, the prediction trajectory of the target can be obtained by introducing these discrete points into the polynomial curve fitting algorithm.

C. UGV Control

In UGV controller, we adopt the method that separates longitudinal and lateral control to prevent coupling and reduce the computational complexity. Specifically, we adopt the "position-speed" cascade control to calculate the vehicle speed $u_{vel}(t)$ for longitudinal tracking, as introduced in [27]. In addition, the LTV-MPC in [28] is employed for lateral control of vehicle tracking due to its low computational complexity [29], [30]. We choose the incremental model to reduce the control mutation. The quadratic programming function with constraints is designed to achieve optimal control for tracking the predicted trajectory as

$$\begin{aligned} \min_{\Delta U(t),\varepsilon} \; & [\Delta U(t), \varepsilon]^T H_t [\Delta U(t), \varepsilon] + f_t [\Delta U(t), \varepsilon] \\ & u_{\min} \le u(t+k) \le u_{\max} \\ & \Delta u_{\min} \le \Delta u(t+k) \le \Delta u_{\max} \\ & k = 0, \cdots, N_c - 1, \end{aligned} \tag{20}$$

where t and k are the current time and discrete control time, ε represents a slack variable, H_t is the quadratic matrix of $\Delta U(t)$, which minimizes tracking errors and control increment, f_t indicates the linear function, $u_{\min}$, $u_{\max}$, $\Delta u_{\min}$, and $\Delta u_{\max}$ denote the minimum and maximum of the control angle and its increments.

In this way, we compute the optimal control increment matrix $\Delta U(t)$. By selecting its first item $\Delta u(t)$ for accumulation, we have the current control angle as $u_{ang}(t) = u_{ang}(t-1) + \Delta u(t)$.

IV. EXPERIMENT

The tracking system comprises a perception subsystem and a UGV, as illustrated in Fig. 1. The perception subsystem is a turntable equipped with RoboSense's 80-line lidar, which helps to expand the scanning range. The UGV utilized was the BIT-Dragon with the independent drive of four wheels and steering of the front and rear, developed by the intelligent perception system team at Beijing Institute of Technology. In the practical procedure, the computers adopted the Robot Operating System (ROS). Furthermore, the DJI Spirit 4pro, a four-rotor UAV, was employed as the tracking target. During the experiment, the drone moved at a speed of 1.0 m/s under crosswind conditions. In these perturbed circumstances, the UAV experienced a maximum lateral drift of 0.33 m within a short time interval. The dynamic tracking procedure of the UGV is depicted in Fig. 3.

The tracking approach is divided into two parts based on the motion trajectory of the drone (red line in Fig. 4). During T = 0 - 20.25 s, the drone experienced significant disturbance from crosswinds, which we refer to as the disturbance

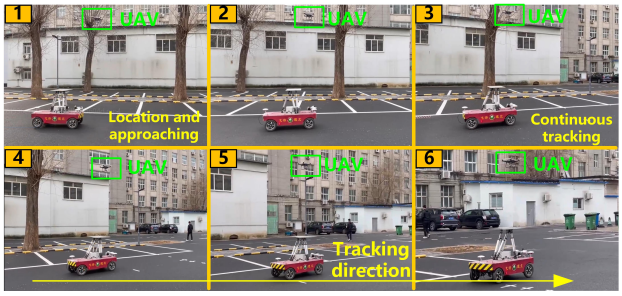

Fig. 3. The scenario of the experiment.

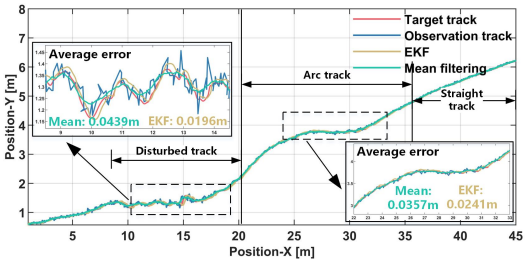

Fig. 4. The results of target estimation.

stage. In this period, the UAV trajectory exhibited noticeable jitter and was accompanied by high-frequency slight noise, particularly at T = 8.75 - 16.05 s. After T = 20.25 s, the motion of the drone experienced fewer disturbances, marking the smooth stage. During this stage, the drone followed a curved trajectory with reduced horizontal jitter, resulting in a smoother movement trajectory.

The absolute position of the target is initially estimated using the EKF, based on the relative localization obtained from the lidar. The target state estimation curve is depicted in Fig. 4. It clearly illustrates that the EKF provides a more effective estimation of the target's position compared to the mean filtering algorithm. Particularly during T = 8.75 - 16.05 s, the mean filtering algorithm exhibits significant issues, including time lag and poor fitting to the rapidly changing curve. In contrast, the EKF reduces the positioning error by 55.4% and 32.5% during the disturbance and smooth stages with less time lag(refer to Table 1). These results indicate that the target location algorithm demonstrates superior real-time capability and positioning accuracy, accurately and robustly estimating the absolute localization of the UAV.

The target trajectory is predicted using the ATP based on UAV positioning. The results are presented in Fig. 5. Fig. 5(a) illustrates the curve prediction at T = 9.65 s. It is evident from both the figure and Table 2 that some prediction algorithms exhibit instability when the target trajectory is severely disturbed. In contrast, the proposed ATP algorithm possesses stronger robustness, achieving more stable predictions. Fig.

TABLE I: Error of positioning.

Algorithm	Error in disturbed stage (m)	Error in smooth stage (m)
Mean filtering	0.0439	0.0357
EKF	0.0196	0.0241

TABLE II: Comparison of different prediction algorithms.

Method	Disturbed trajectory			Smooth trajectory		
	Average error (mm)	Root mean square error (mm)	Maximum error (mm)	Average error (mm)	Root mean square error (mm)	Maximum error (mm)
Quintic polynomial fitting (Unstable)	-153.69	$1.36 * 10^3$	$1.34 * 10^4$	15.67	721.40	$3.71 * 10^3$
Kalman filter	28.61	71.15	395.19	-3.96	26.59	110.23
CV	28.22	62.31	318.61	-10.63	31.74	111.72
CLAV	20.02	89.86	643.60	9.82	34.66	221.10
ATP (Own)	26.07	57.38	318.61	-0.83	27.35	93.30

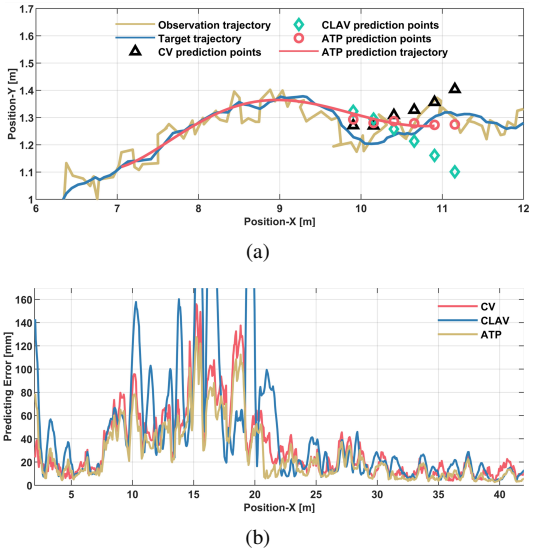

Fig. 5. The results of target prediction: (a) Prediction trajectory; (b) Prediction error.

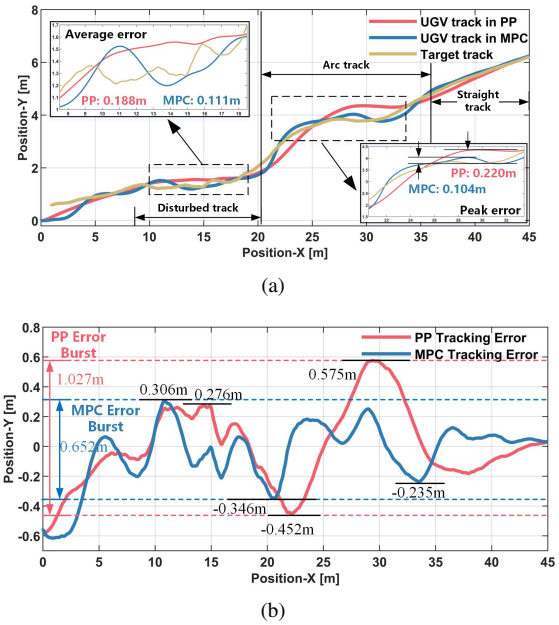

Fig. 6. The results of target tracking: (a) Tracking trajectory; (b) Tracking error in Y direction.

5(b) compares the absolute prediction error of the CV, CLAV, and ATP. We can see that the ATP has higher prediction accuracy on the whole track by adjusting the weight adaptively. Among them, in the disturbed trajectory, ATP is closer to the CV recursive algorithm with high prediction stability. While at the smooth stage, it approaches the CLAV with accurate curve prediction. In addition, the detailed data comparison in two stages is shown in Table 2. It can be seen from the table that the average error, root mean square error, and maximum error of ATP are the comprehensively smallest compared with other prediction algorithms. In conclusion, the proposed ATP algorithm can predict target trajectories with the highest accuracy and the best robustness under different stages and conditions, providing a stable reference for UGV tracking.

Eventually, the LTV-MPC is employed for UGV tracking. The UGV trajectory and the tracking error are shown in Fig. 6(a) and Fig. 6(b). The Pure Pursuit (PP) tracking algorithm is selected for tracking comparison. It can be seen from the figure that the UGV in MPC is closer to the UAV's actual positioning than in PP. Under the disturbed and smooth trajectories, the MPC tracking algorithm reduces the tracking error by 41.0% and 52.7%. In addition, with the characteristics of control increment limiting, UGV in MPC has smaller motion mutations than PP. We can conclude that the tracking algorithm based on LTV-MPC has higher control accuracy and achieves stable tracking of the predicted trajectory of the target.

We have proved the reliability of the system's state estimation, trajectory prediction, and dynamic tracking to the target under multi-disturbed conditions through three stages of experiments. The UGV finally tracks the mobile target drone at a speed of 1.0 m/s stably.

V. CONCLUSION

In this paper, we present a trajectory-prediction-based dynamic tracking scheme for multi-disturbed conditions. Specifically, the EKF is employed to estimate the target's position under detection noise and frame rate fluctuations. Additionally, we propose the ATP algorithm based on state-recursive anchors to predict the trajectory of the target with unknown disturbances. Experimental results demonstrate that ATP exhibits superior disturbance rejection and prediction accuracy compared to other algorithms. Lastly, the LTV-MPC is utilized for UGV tracking. Experimental results validate the effectiveness of the proposed trajectory-prediction-based tracking scheme for dynamically tracking moving targets under multiple disturbance conditions.

VI. ACKNOWLEDGEMENT

This work is supported by National Natural Science Foundation of China under Grant No.61773060.

REFERENCES

[1] S. Wang, F. Jiang, B. Zhang, R. Ma, and Q. Hao, "Development of uav-based target tracking and recognition systems," *IEEE Transactions on Intelligent Transportation Systems*, vol. 21, no. 8, pp. 3409–3422, 2019.

[2] Y. Wang, C. Tang, S. Wang, L. Cheng, R. Wang, M. Tan, and Z. Hou, "Target tracking control of a biomimetic underwater vehicle through deep reinforcement learning," *IEEE Transactions on Neural Networks and Learning Systems*, vol. 33, no. 8, pp. 3741–3752, 2021.

[3] M. Chen, H. Ma, Y. Kang, and Q. Wu, "Adaptive neural safe tracking control design for a class of uncertain nonlinear systems with output constraints and disturbances," *IEEE Transactions on Cybernetics*, vol. 52, no. 11, pp. 12 571–12 582, 2021.

[4] Y. Song and J. Guo, "Neuro-adaptive fault-tolerant tracking control of lagrange systems pursuing targets with unknown trajectory," *IEEE Transactions on Industrial Electronics*, vol. 64, no. 5, pp. 3913–3920, 2016.

[5] N. Li, C. Lu, X. Yu, X. Liu, and B. Su, "Real-time 3d-lidar, mmw radar and gps/imu fusion based vehicle detection and tracking in unstructured environment," in *2021 IEEE International Conference on Robotics and Automation (ICRA)*. IEEE, 2021, pp. 13 339–13 345.

[6] P. Sun, B. Zhu, Z. Zuo, and M. V. Basin, "Vision-based finite-time uncooperative target tracking for uav subject to actuator saturation," *Automatica*, vol. 130, p. 109708, 2021.

[7] D. Chwa, "Robust nonlinear disturbance observer based adaptive guidance law against uncertainties in missile dynamics and target maneuver," *IEEE Transactions on Aerospace and Electronic Systems*, vol. 54, no. 4, pp. 1739–1749, 2018.

[8] W. D. Blair and Y. Bar-Shalom, "Mse design of nearly constant velocity kalman filters for tracking targets with deterministic maneuvers," *IEEE Transactions on Aerospace and Electronic Systems*, vol. 59, no. 4, pp. 4180 – 4191, 2023.

[9] M. Wang, K. Y. Leung, R. Liu, S. Song, Y. Yuan, J. Yin, M. Q.-H. Meng, and J. Liu, "Dynamic tracking for microrobot with active magnetic sensor array," in *2021 IEEE International Conference on Robotics and Automation (ICRA)*. IEEE, 2021, pp. 7288–7294.

[10] W. Zhang, M. Tognon, L. Ott, R. Siegwart, and J. Nieto, "Active model learning using informative trajectories for improved closed-loop control on real robots," in *2021 IEEE International Conference on Robotics and Automation (ICRA)*. IEEE, 2021, pp. 4467–4473.

[11] L. Sun, H. Cao, and Y. Song, "Prescribed performance control of constrained euler-language systems chasing unknown targets," *IEEE Transactions on Cybernetics*, vol. 53, no. 8, pp. 4829 – 4840, 2022.

[12] X. Cao, L. Ren, and C. Sun, "Dynamic target tracking control of autonomous underwater vehicle based on trajectory prediction," *IEEE Transactions on Cybernetics*, vol. 53, no. 3, pp. 1968–1981, 2022.

[13] L. Zhang, P. Li, J. Chen, and S. Shen, "Trajectory prediction with graph-based dual-scale context fusion," in *2022 IEEE/RSJ International Conference on Intelligent Robots and Systems (IROS)*. IEEE, 2022, pp. 11 374–11 381.

[14] Q. Wang, Y. Gao, J. Ji, C. Xu, and F. Gao, "Visibility-aware trajectory optimization with application to aerial tracking," in *2021 IEEE/RSJ International Conference on Intelligent Robots and Systems (IROS)*. IEEE, 2021, pp. 5249–5256.

[15] J. Strohbeck, J. Müller, M. Herrmann, and M. Buchholz, "Deep kernel learning for uncertainty estimation in multiple trajectory prediction networks," in *2022 IEEE/RSJ International Conference on Intelligent Robots and Systems (IROS)*. IEEE, 2022, pp. 11 396–11 402.

[16] M. Wang, Y. Liu, D. Su, Y. Liao, L. Shi, J. Xu, and J. V. Miro, "Accurate and real-time 3-d tracking for the following robots by fusing vision and ultrasonar information," *IEEE/ASME Transactions On Mechatronics*, vol. 23, no. 3, pp. 997–1006, 2018.

[17] P. Paral, A. Chatterjee, A. Rakshit, and S. K. Pal, "Extended target tracking in human–robot coexisting environments via multisensor information fusion: A heteroscedastic gaussian process regression based approach," *IEEE Transactions on Industrial Informatics*, vol. 19, no. 9, pp. 9877 – 9886, 2023.

[18] G. Li, G. Li, and Y. He, "Resolvable group target tracking via multi-bernoulli filter and its application to sensor control scenario," *IEEE Transactions on Signal Processing*, vol. 70, pp. 6286–6299, 2022.

[19] Y. Ji, X. Hu, Y. Chen, Y. Mao, G. Wang, Q. Li, and J. Zhang, "Model-based trajectory prediction and hitting velocity control for a new table tennis robot," in *2021 IEEE/RSJ International Conference on Intelligent Robots and Systems (IROS)*. IEEE, 2021, pp. 2728–2734.

[20] N. P. Bhatt, A. Khajepour, and E. Hashemi, "Mpc-pf: Social interaction aware trajectory prediction of dynamic objects for autonomous driving using potential fields," in *2022 IEEE/RSJ International Conference on Intelligent Robots and Systems (IROS)*. IEEE, 2022, pp. 9837–9844.

[21] Z. Shao, Y. Wang, and X. Chen, "Global prescribed performance control for strict feedback systems pursuing uncertain target," *IEEE Transactions on Neural Networks and Learning Systems*, vol. 35, no. 2, pp. 2403 – 2412, 2022.

[22] J. Ruiping, Y. Liang, X. Linfeng, and W. Zhenwei, "Trajectory prediction of ballistic missiles using gaussian process error model," *Chinese Journal of Aeronautics*, vol. 35, no. 1, pp. 458–469, 2022.

[23] K. Li, Y. Han, X. Yan *et al.*, "Distributed multi-uav cooperation for dynamic target tracking optimized by an saqpso algorithm," *ISA transactions*, vol. 129, pp. 230–242, 2022.

[24] G. Xie and X. Chen, "Efficient and robust online trajectory prediction for non-cooperative unmanned aerial vehicles," *Journal of Aerospace Information Systems*, vol. 19, no. 2, pp. 143–153, 2022.

[25] T. Keviczky, P. Falcone, F. Borrelli, J. Asgari, and D. Hrovat, "Predictive control approach to autonomous vehicle steering," in *2006 American control conference*. IEEE, 2006, pp. 6–pp.

[26] H. Berkemeyer, R. Franceschini, T. Tran, L. Che, and G. Pipa, "Feasible and adaptive multimodal trajectory prediction with semantic maneuver fusion," in *2021 IEEE International Conference on Robotics and Automation (ICRA)*. IEEE, 2021, pp. 8530–8536.

[27] G. Zhang, Y. He, B. Dai, F. Gu, L. Yang, J. Han, G. Liu, and J. Qi, "Grasp a moving target from the air: System & control of an aerial manipulator," in *2018 IEEE International Conference on Robotics and Automation (ICRA)*. IEEE, 2018, pp. 1681–1687.

[28] P. Falcone, F. Borrelli, H. E. Tseng, J. Asgari, and D. Hrovat, "Linear time-varying model predictive control and its application to active steering systems: Stability analysis and experimental validation," *International Journal of Robust and Nonlinear Control: IFAC-Affiliated Journal*, vol. 18, no. 8, pp. 862–875, 2008.

[29] X. Gong, S. Liang, B. Wang, and W. Zhang, "Game theory-based decision-making and iterative predictive lateral control for cooperative obstacle avoidance of guided vehicle platoon," *IEEE Transactions on Vehicular Technology*, vol. 72, no. 6, pp. 7051 – 7066, 2023.

[30] W. Y. Choi, S.-H. Lee, and C. C. Chung, "Horizonwise model-predictive control with application to autonomous driving vehicle," *IEEE transactions on industrial informatics*, vol. 18, no. 10, pp. 6940–6949, 2021.